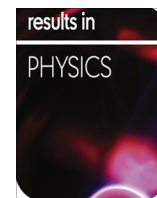


Contents lists available at [ScienceDirect](http://ScienceDirect.com)

## Results in Physics

journal homepage: [www.journals.elsevier.com/results-in-physics](http://www.journals.elsevier.com/results-in-physics)

# Framing the features of Brownian motion and thermophoresis on radiative nanofluid flow past a rotating stretching sheet with magnetohydrodynamics

F. Mabood<sup>a,\*</sup>, S.M. Ibrahim<sup>b</sup>, W.A. Khan<sup>c</sup><sup>a</sup> Department of Mathematics, University of Peshawar, 25120, Pakistan<sup>b</sup> Department of Mathematics, GITAM University, Visakhapatnam, Andhra Pradesh 530045, India<sup>c</sup> Department of Mechanical and Industrial Engineering, Majmaah University, Majmaah 11952, Saudi Arabia

## ARTICLE INFO

## Article history:

Received 27 September 2016

Received in revised form 17 November 2016

Accepted 19 November 2016

Available online 22 November 2016

## Keywords:

Nanofluid

MHD

Chemical reaction

Rotating stretching sheet

Radiation

## ABSTRACT

This article addresses the combined effects of chemical reaction and viscous dissipation on MHD radiative heat and mass transfer of nanofluid flow over a rotating stretching surface. The model used for the nanofluid incorporates the effects of the Brownian motion and thermophoresis in the presence of heat source. Similarity transformation variables have been used to model the governing equations of momentum, energy, and nanoparticles concentration. Runge-Kutta-Fehlberg method with shooting technique is applied to solve the resulting coupled ordinary differential equations. Physical features for all pertinent parameters on the dimensionless velocity, temperature, skin friction coefficient, and heat and mass transfer rates are analyzed graphically. The numerical comparison has also presented for skin friction coefficient and local Nusselt number as a special case for our study. It is noted that fluid velocity enhances when rotational parameter is increased. Surface heat transfer rate enhances for larger values of Prandtl number and heat source parameter while mass transfer rate increases for larger values of chemical reaction parameter.

© 2016 Published by Elsevier B.V. This is an open access article under the CC BY-NC-ND license (<http://creativecommons.org/licenses/by-nc-nd/4.0/>).

## Introduction

The study of boundary layer flow and heat transfer over a stretching sheet has many important industrial and technological applications such as materials manufactured by polymer extrusion, drawing of copper wires, continuous stretching of plastic films, artificial fibres, hot rolling, wire drawing, etc. In these cases, the final product of desired characteristics depends on the rate of cooling in the process and the process of stretching. Crane [1] investigated the steady two-dimensional boundary layer flow caused by the stretching of the sheet which moves in its own plane at a velocity that varies linearly with the distance from the slit. Later many researchers extended this problem to the Newtonian and non-Newtonian fluids under various physical conditions. Gupta and Gupta [2] studied the heat and mass transfer characteristics with suction or blowing. Rajagopal et al. [3] analysed the characteristics of the boundary layer flow for small values of viscoelastic parameter and showed that the skin friction coefficient decreases with

the increase of viscoelastic parameter. Char [4] discussed the effects of magnetic field and power law surface temperature on heat and mass transfer from a continuous flat surface.

The problems of heat and mass transfer in combination with radiation are of great importance in manufacturing industries for the design of fins, steel rolling, nuclear power plants, and gas turbines and various propulsion devices for aircraft, missiles, satellites and space vehicles, etc. The radiative flow of an electrically conducting fluid with high temperature in the presence of magnetic field occurs in electrical power generations, astrophysical flows, solar power technology, etc. Raptis [5] studied the role of radiation in a viscoelastic fluid flow. Abd El-Aziz [6] analyzed the effect of radiation on the unsteady flow and heat transfer over stretching surface. Thermal radiation effects on heat and mass transfer over a stretching sheet was investigated by Shateyi and Motsa [7].

Changes in fluid density gradients may be caused by nonreversible chemical reaction in the system as well as by differences in the molecular weight between values of the reactants and the products. Apelblat [8] studied analytical solution for mass transfer with chemical reaction of the first order. Chemical reaction effects on MHD heat and mass transfer flow over a stretching surface in a porous medium was studied by Cortell [9]. Anjalidevi et al.

\* Corresponding author.

E-mail addresses: [mabood1971@yahoo.com](mailto:mabood1971@yahoo.com) (F. Mabood), [ibrahimsvu@gmail.com](mailto:ibrahimsvu@gmail.com) (S.M. Ibrahim), [wkhan1956@gmail.com](mailto:wkhan1956@gmail.com) (W.A. Khan).

[10] have examined the effect of chemical reaction on the flow in the presence of heat transfer and magnetic field. Ibrahim et al. [11] obtained the combined effects of a transverse magnetic field and radiation on an unsteady mass transfer flow with chemical reaction through a channel filled with saturated porous medium and non-uniform wall temperature, Mabood et al. [12] reported the effects of chemical reaction on MHD stagnation point flow past a stretching sheet with heat transfer analysis.

Viscous dissipation effect plays an important role in many practical applications such as oil products transportation through ducts, polymer processing, etc. Generally, this effect is characterised by the Eckert number. Grebhart and Mollendorf [13] obtained the explicit calculation of the viscous dissipation in a multi-dimensional natural convection flow over an infinite flat vertical surface. Vajravelu and Hadjinicolaou [14] obtained the analytical results for the heat transfer in viscous fluid flow over a stretching surface with viscous dissipation and heat generation. Wahiduzzaman et al. [15] analyzed the viscous dissipation and radiation effects on MHD boundary layer flow of a nanofluid over a rotating stretching sheet.

“Nanofluid” is the name conceived to describe a fluid in which nanometer-sized particles are suspended. Due to small size and very large specific surface areas of nanoparticles, nanofluids have superior properties like high thermal conductivity, minimal clogging in flow passages, long-term stability and homogeneity which make them potentially useful in many applications in heat transfer including microelectronic, solar energy, nuclear reactors, pharmaceutical processes, hybrid-powered engines, etc. Choi [16] was mostly the first researcher to introduce the technique of nanofluids by using a mixture of nanoparticles and the base fluids. Buongiorno [17] showed that such massive increase in the thermal conductivity occurs due to the presence of two main effects namely the Brownian diffusion and the thermophoretic diffusion of nanoparticles. Mabood et al. [18] focused on the study of combined heat and mass transfer of electrically conducting nanofluid over a non-linear stretching surface in the presence of a first-order chemical reaction and viscous dissipation. Rana and Bhargava [19] numerically investigated the flow of nanofluid over a nonlinearly stretching sheet using finite element method. Kumar [20] investigated the radiative heat transfer with the viscous dissipation effect in the presence of transverse magnetic field. Ramana Reddy et al. [21] studied the behaviour of MHD nanofluid flow past a permeable plate in porous medium under the influence of chemical reaction, radiation and rotation. Some relevant studies can be found from the list of Refs. [27–33].

Motivated by the investigation mentioned above, the aim of the present work is to investigate the effects of viscous dissipation and heat source on chemically radiative MHD boundary layer flow of a nanofluid past a rotating stretching sheet. The nonlinearity of basic equations associated with their inherent mathematical difficulties has led us to use numerical method. Thus the transformed dimensionless governing equations are solved numerically by using the Runge–Kutta–Fehlberg method (RKF) method along with shooting technique. It is hoped that the results obtained from the present study will provide useful information for different industrial applications. To the best of our best knowledge such a study is not investigated in the scientific literature.

## 2. Mathematical formulation

We consider a two-dimensional steady boundary layer flow of an incompressible, electrically conducting nanofluid past a stretching surface of a rotating system with the linear stretching velocity  $u_w = ax$ . Fluid flows over the region of  $y \geq 0$ . The x-axes and y-axes are taken respectively in the direction along and perpendicular to

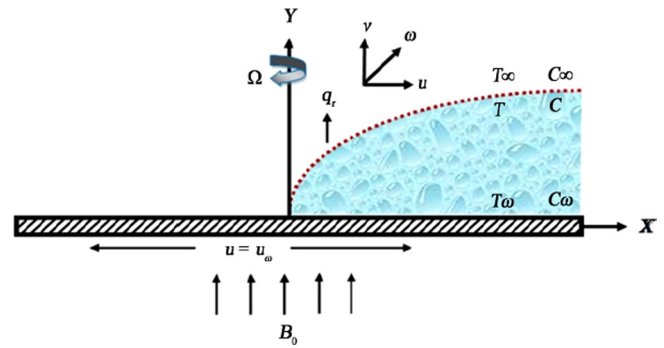


Fig. 1. Physical model.

the fluid motion (see Fig. 1). It is assumed that at the stretching surface, the temperature  $T$  and the concentration  $C$  takes constant value  $T_w$  and  $C_w$  respectively. The ambient values attained as  $y$  tends to infinity of  $T$  and  $C$  are denoted by  $T_\infty$  and  $C_\infty$  respectively. The flow field is exposed to the influence of an external transverse magnetic field of  $B = (0, B_0, 0)$ . The governing equations of the flow are given by Khan and Pop [21]

$$\frac{\partial u}{\partial x} + \frac{\partial v}{\partial y} = 0 \quad (1)$$

$$u \frac{\partial u}{\partial x} + v \frac{\partial u}{\partial y} = U \frac{dU}{dx} + \nu \frac{\partial^2 u}{\partial y^2} + 2\Omega w + \frac{\sigma B_0^2}{\rho} (U - u) \quad (2)$$

$$u \frac{\partial w}{\partial x} + v \frac{\partial w}{\partial y} = \nu \frac{\partial^2 w}{\partial y^2} - 2\Omega w - \frac{\sigma B_0^2 w}{\rho} \quad (3)$$

$$u \frac{\partial T}{\partial x} + v \frac{\partial T}{\partial y} = \alpha \frac{\partial^2 T}{\partial y^2} - \frac{\alpha}{k} \left( \frac{\partial q_r}{\partial y} \right) + \frac{Q_0}{\rho C_p} (T - T_\infty) + \frac{v}{C_p} \left( \frac{\partial u}{\partial y} \right)^2 + \tau \left[ D_B \left( \frac{\partial C}{\partial y} \cdot \frac{\partial T}{\partial y} \right) + \frac{D_T}{T_\infty} \left( \frac{\partial T}{\partial y} \right)^2 \right] \quad (4)$$

$$u \frac{\partial C}{\partial x} + v \frac{\partial C}{\partial y} = D_B \frac{\partial^2 C}{\partial y^2} + \frac{D_T}{T_\infty} \frac{\partial^2 T}{\partial y^2} - k_r (C - C_\infty) \quad (5)$$

The boundary conditions for the velocity, temperature and concentration fields are

$$\begin{aligned} u &= u_w = ax, v = 0, w = 0, T = T_w = T_\infty + A_1 \left( \frac{x}{l} \right)^m, \\ C &= C_w = C_\infty + A_2 \left( \frac{x}{l} \right)^m, \quad \text{at } y = 0. \\ u &= U = bx, w = 0, T \rightarrow T_\infty, C \rightarrow C_\infty, \quad \text{as } y \rightarrow \infty \end{aligned} \quad (6)$$

where  $u, v, w$  are velocity components,  $\alpha = \frac{k}{\rho C_p}$  is the thermal diffusivity,  $\rho$  is density,  $C_p$  is specific heat at constant,  $k$  is the thermal conductivity,  $\sigma$  is the electrical conductivity,  $U$  is the uniform velocity,  $a$  and  $b$  the linear constant parameter,  $l$  is the characteristics length and  $A_1, A_2$ , is the constant whose values depends on the properties of the fluid,  $m$  is the constant parameter.

$D_B$  is the Brownian diffusion coefficient,  $D_T$  is the thermophoretic diffusion coefficient,  $\tau$  Effective heat capacity of nano particle  $Q$  is the temperature dependent volumetric rate of heat source  $q_r$  is the radiative heat term,  $k_r$  is the dimensioned chemical reaction parameter.

The stream function satisfying Eq. (1) is defined as  $u = \frac{\partial \psi}{\partial y}$  and  $v = -\frac{\partial \psi}{\partial x}$ . Defining the following similarity transformation variables:

$$\begin{aligned} \eta &= y\sqrt{\frac{a}{\nu}}, \psi = x\sqrt{av}f(\eta), g_0(\eta) = \frac{w}{U}, \theta = \theta(\eta) \\ &= \frac{T - T_\infty}{T_w - T_\infty}, \phi = \phi(\eta) = \frac{C - C_\infty}{C_w - C_\infty} \\ u &= \frac{\partial\psi}{\partial y}, \quad v = -\frac{\partial\psi}{\partial x} \end{aligned} \tag{7}$$

Using Eq. (7), the governing partial differential equations are reduced to

$$f''' + ff'' - f'^2 + M(\lambda - f') + 2R'g + \lambda^2 = 0 \tag{8}$$

$$g'' + fg' - 2R'f' + Mg = 0 \tag{9}$$

$$(1 + R)\theta'' + EcPrf'^2 + Prf'\theta' - mPrf'\theta + PrNb\theta'\phi' + PrNt\theta^2 + PrQ\theta = 0 \tag{10}$$

$$\phi'' + Lef\phi' + \frac{Nt}{Nb}\theta'' - Lemf'\phi - \gamma ReLe\phi = 0 \tag{11}$$

The transformed boundary conditions are as follows:

$$f = 0, \quad f' = 1, \quad g_0 = 0, \quad \theta = 1, \quad \phi = 1 \quad \text{at } \eta = 0 \tag{12}$$

$$f' = \lambda, \quad g = 0, \quad \theta = 0, \quad \phi = 0 \quad \text{as } \eta \rightarrow \infty$$

Here  $M = \frac{\sigma B_0^2}{\rho a}$  is the magnetic parameter,  $R = \frac{16\sigma_s T_\infty^3}{3k\kappa^*}$  is the radiation parameter  $Pr = \frac{\nu}{\alpha}$  is the Prandtl number,  $Ec = \frac{u_\infty^2}{C_p(T_w - T_\infty)}$  is the Eckert number,  $R' = \frac{\Omega x}{U^2}$  is the rotational parameter,  $Q = \frac{Q_0 x}{\rho C_p a U}$  is the heat source parameter,  $Le = \frac{\nu}{D_B}$  is the Lewis number,  $Nb = \frac{(\rho C)_p D_B (C_w - C_\infty)}{\nu(\rho C)_f}$  is the Brownian motion parameter,  $Nt = \frac{(\rho C)_p D_T (T_w - T_\infty)}{\nu T_\infty (\rho C)_f}$  is the thermophoresis parameter,  $\gamma = \frac{k_r U (C_w - C_\infty)}{\nu T_\infty (\rho C)_f}$  is the chemical reaction parameter,  $\lambda = b/a$  is the stretching parameter and  $m$  is constant.

The physical quantities of interest for the governing flow problem are skin-friction coefficient, the reduced Nusselt number and reduced Sherwood number, which can be written as [23–24]

$$C_f(Re_x)^{\frac{1}{2}} = -f''(0) \tag{13}$$

$$C_g(Re_x)^{\frac{1}{2}} = -g'(0) \tag{14}$$

$$Nu(Re_x)^{\frac{1}{2}} = -\theta'(0) \tag{15}$$

$$Sh(Re_x)^{\frac{1}{2}} = -\phi'(0) \tag{16}$$

where  $Re_x = \frac{Ux}{\nu}$  is the Reynolds number.

### 3. Solution method

The reduced Eqs. (8)–(11) are nonlinear and coupled, and thus their exact analytical solutions is not possible. These equations are solved numerically using Runge-Kutta-Fehlberg method with shooting technique for different values of parameters. The effects

of the emerging parameters on the dimensionless velocity, temperature, skin friction coefficient, the rate of heat and mass transfer are investigated. The step size and convergence criteria were chosen to be 0.001 and  $10^{-6}$  respectively. The asymptotic boundary conditions in Eq. (6) were approximated by using a value of 10 for  $\eta_{max}$  as follows:

$$\eta_{max} = 10, f'(10) = \lambda, g(10) = 0, \theta(10) = 0, \phi(10) = 0. \tag{17}$$

This ensures that all numerical solutions approached the asymptotic values correctly.

To validate the obtained solution, comparisons have been made with previously published data from the literature for  $-f''(0)$  and  $-\theta'(0)$  in Tables 1–3, and they are found to be in a favorable agreement.

### 4. Results and discussion

The heat and mass transfer characteristics in nanofluid flow due to a stretching sheet subjected of a rotating system subjected to various parameters like magnetic parameter  $M$ , radiation parameter  $R$ , Prandtl number  $Pr$ , Eckert number  $Ec$ , rotational parameter  $R'$ , Lewis number  $Le$ , Brownian motion parameter  $Nb$ , Thermophoresis parameter  $Nt$ , stretching parameter  $\lambda$ , Constant parameter  $m$ , heat source parameter  $Q$ , chemical reaction parameter  $\gamma$  have been studied numerically. For illustration of the results, numerical values are plotted in Figs. 1–12.

Fig. 2(a) shows the effect of magnetic parameter  $M$  on primary velocity. As the magnetic parameter  $M$  increases, the velocity decreases. This is due to the fact that, an increase in the strength of magnetic field produces a resistive force called Lorentz force which reduces the fluid velocity. Effect of rotational parameter  $R'$  on primary velocity is shown in Fig. 2(b). As shown in the figure primary velocity decreases with the increase of rotational parameter  $R'$ .

**Table 2**  
Comparison of  $-\theta'(0)$  when  $M = 1, R' = \lambda = R = Ec = m = Q = Nb = Nt = 0$ .

Pr	Sreenivasulu and Reddy [25]	Hamad and Pop [26]	Present results
0.7	0.45395	0.45391	0.4544
2	0.91131	0.91136	0.9113
7	1.89541	1.89540	1.8954
20	3.35390	3.39350	3.3539
70	6.46221	6.46220	6.4622

**Table 3**  
Comparison of  $-\theta'(0)$  when  $Pr = Le = 10, R' = \lambda = R = Ec = M = m = Q = 0$ .

Nb = Nt	Khan and Pop [22]	Present results
0.1	0.9524	0.95237
0.2	0.3654	0.36536
0.3	0.1355	0.13551
0.4	0.0495	0.04946
0.5	0.0179	0.01792

**Table 1**  
Comparison of  $-f''(0)$  and  $-\theta'(0)$  for different values of  $Q$  &  $M$  when  $R' = \lambda = R = Ec = Nb = Nt = 0, Pr = m = 1$ .

Q	Mabood et al. [18]				Present results			
	M = 5		M = 10		M = 5		M = 10	
	$-f''(0)$	$-\theta'(0)$	$-f''(0)$	$-\theta'(0)$	$-f''(0)$	$-\theta'(0)$	$-f''(0)$	$-\theta'(0)$
-0.2	2.44949	0.88444	3.31662	0.80175	2.44948	0.88444	3.31663	0.80175
0.0	2.44949	0.67051	3.31662	0.54649	2.44948	0.67051	3.31663	0.54649
0.2	2.44949	0.75900	3.31662	0.58855	2.44948	0.75900	3.31663	0.58855

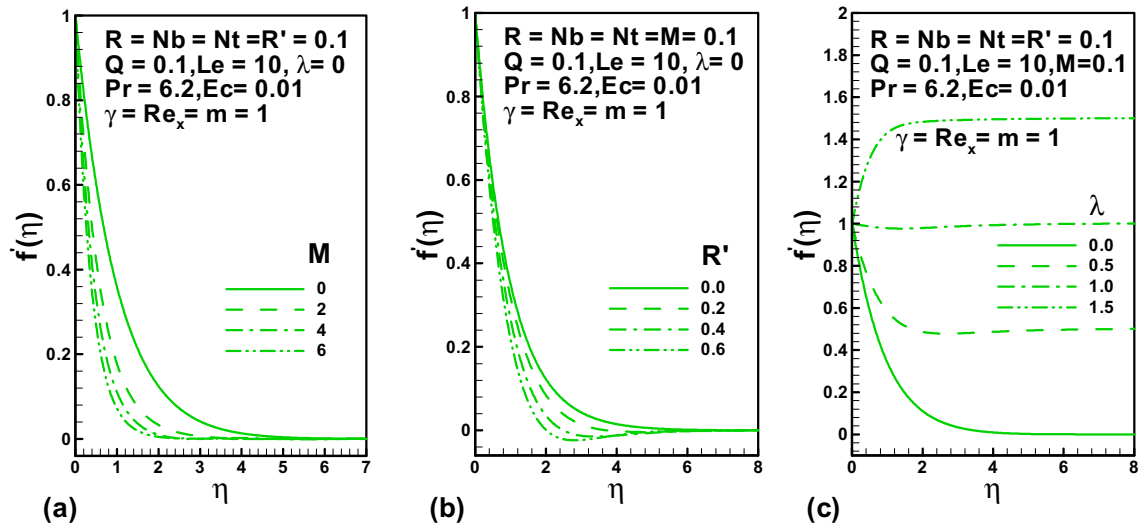


Fig. 2. Effects of  $M$ ,  $R'$  &  $\lambda$  on  $f'(\eta)$ .

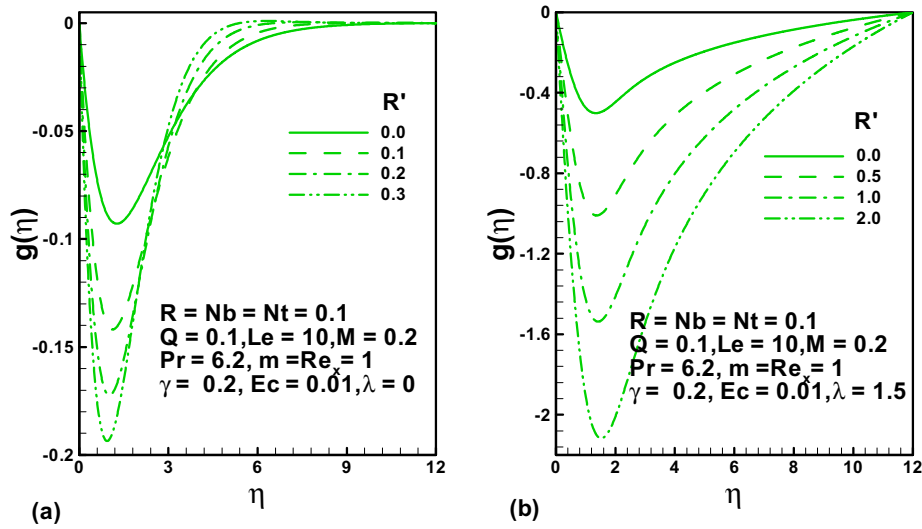


Fig. 3. Effects of  $R'$  on  $g(\eta)$  for (a)  $\lambda = 0$  and for (b)  $\lambda = 1.5$ .

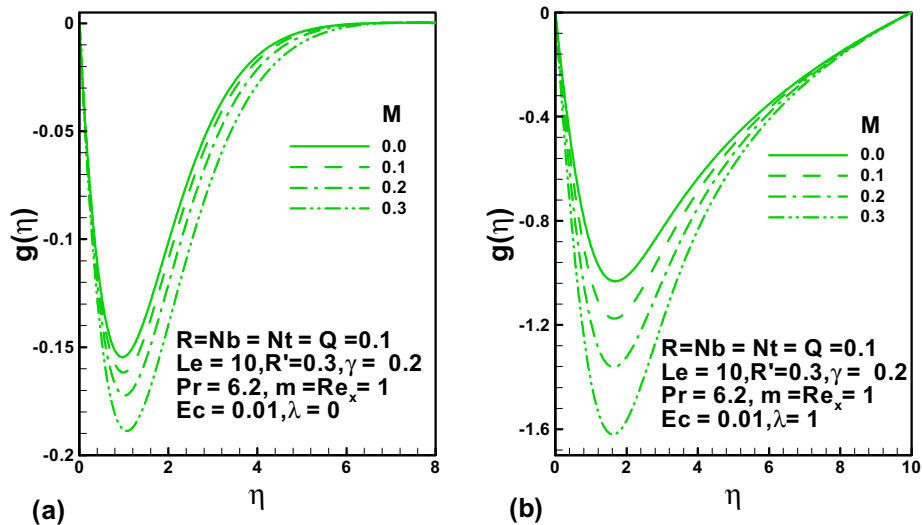


Fig. 4. Effects of  $M$  on  $g(\eta)$  for (a)  $\lambda = 0$  and for (b)  $\lambda = 1$ .

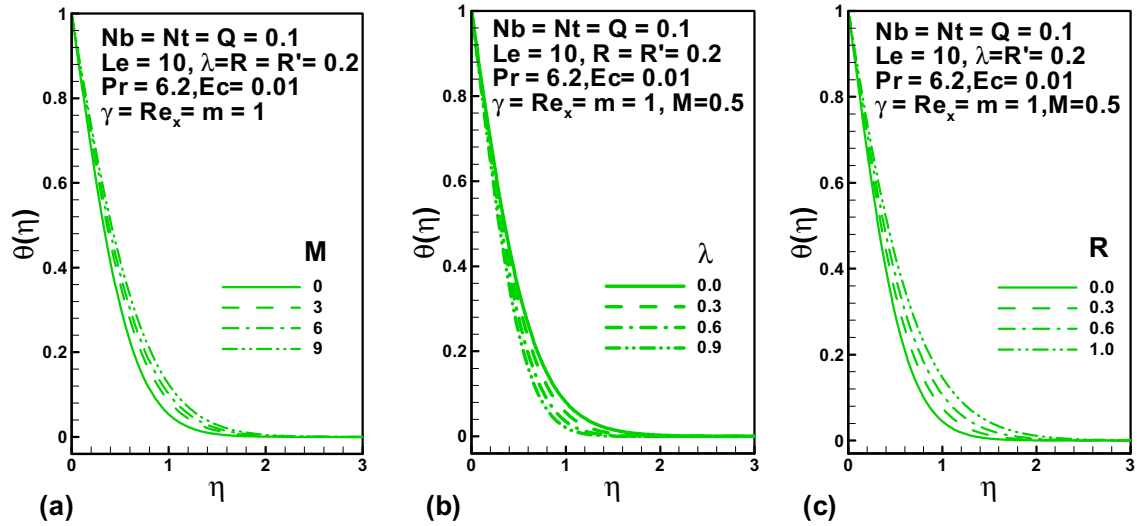


Fig. 5. Effects of  $M$ ,  $\lambda$  &  $R$  on  $\theta(\eta)$ .

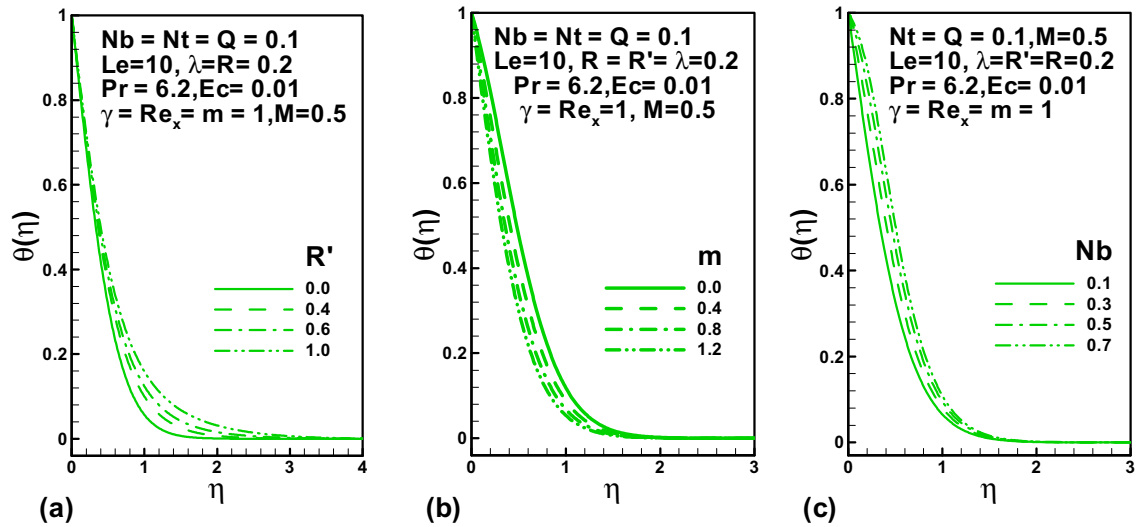


Fig. 6. Effects of  $R'$ ,  $m$  &  $Nb$  on  $\theta(\eta)$ .

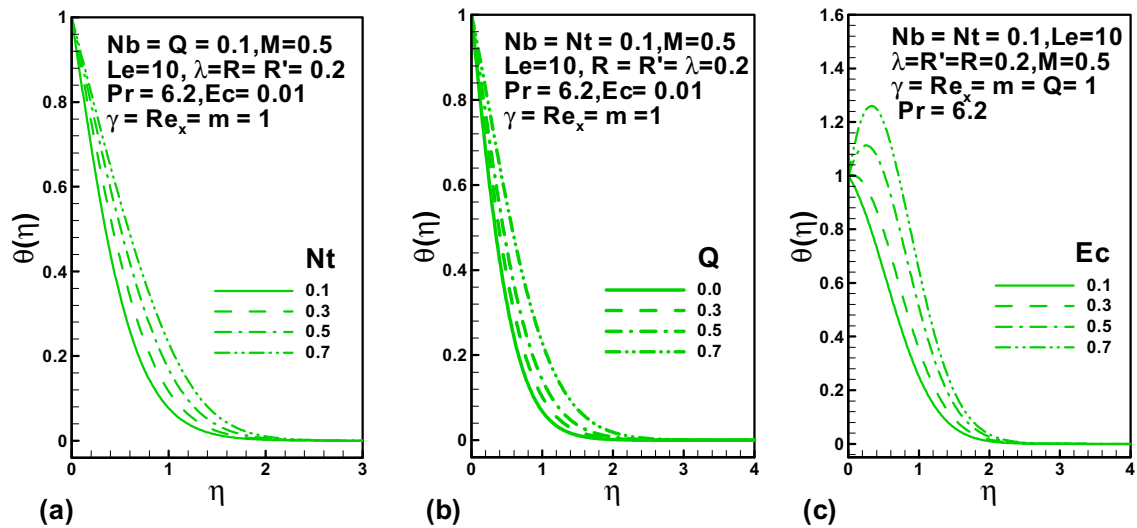


Fig. 7. Effects of  $Nt$ ,  $Q$  &  $Ec$  on  $\theta(\eta)$ .

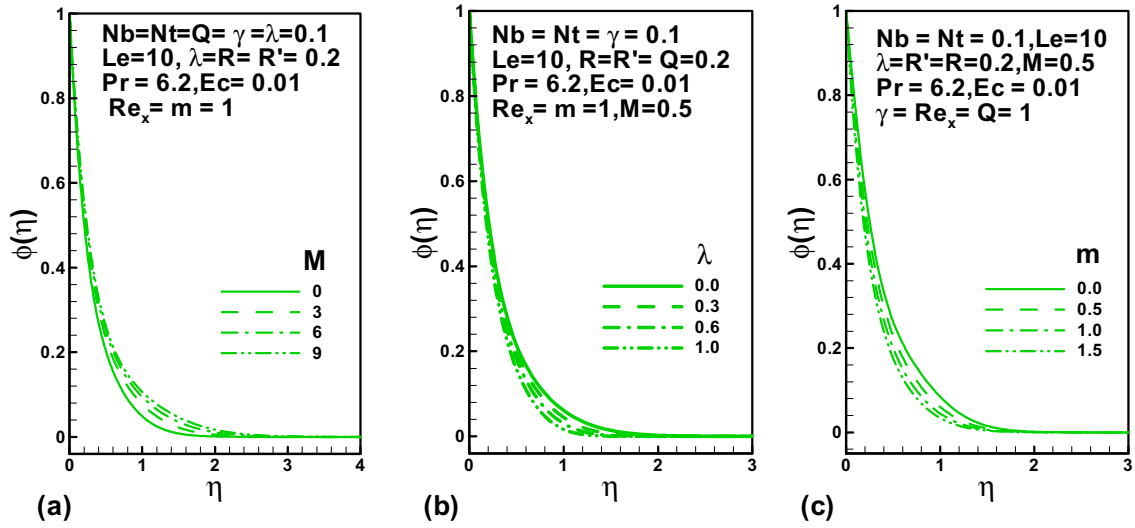


Fig. 8. Effects of  $M$ ,  $\lambda$  &  $m$  on  $\phi(\eta)$ .

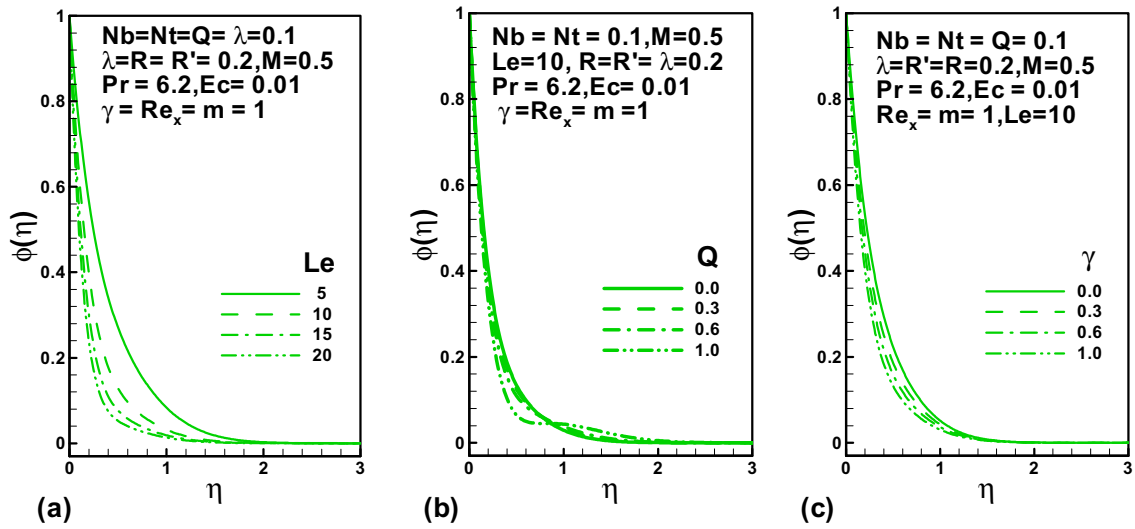


Fig. 9. Effects of  $Le$ ,  $Q$  &  $\gamma$  on  $\phi(\eta)$ .

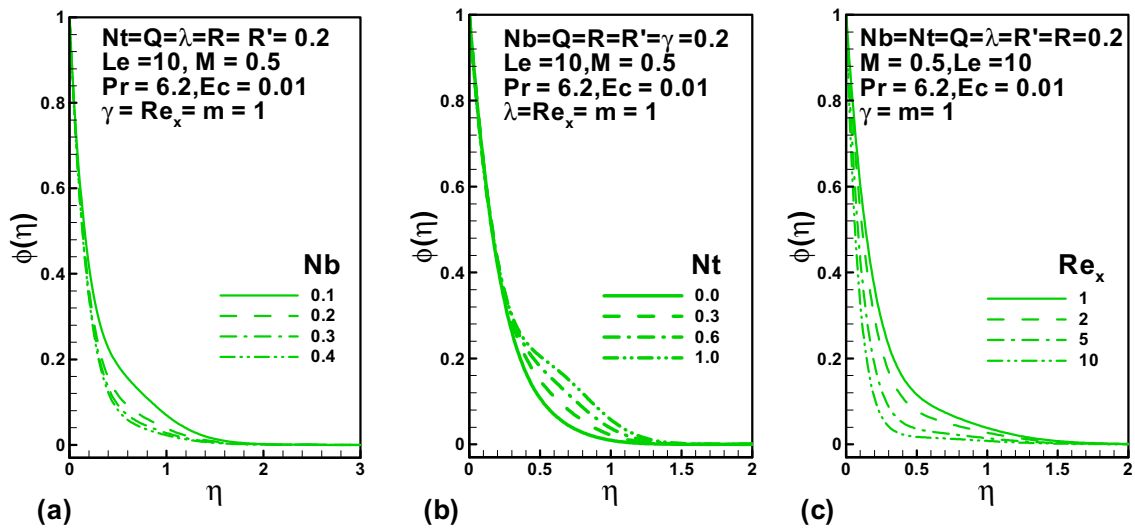


Fig. 10. Effects of  $Nb$ ,  $Nt$  &  $Re_x$  on  $\phi(\eta)$ .

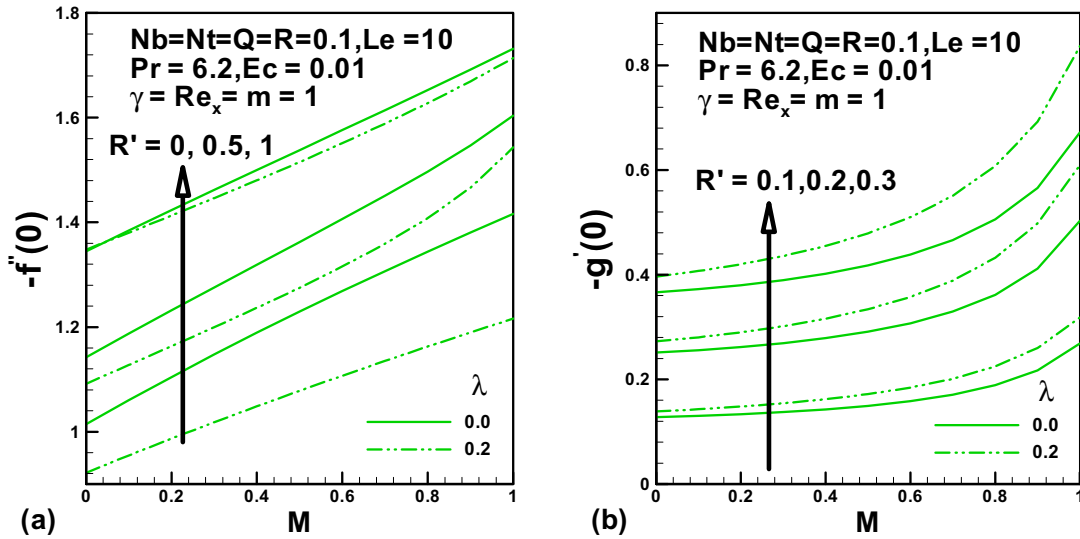


Fig. 11. Effects of  $M$ ,  $R'$  &  $\lambda$  on  $-f''(0)$  &  $-g'(0)$ .

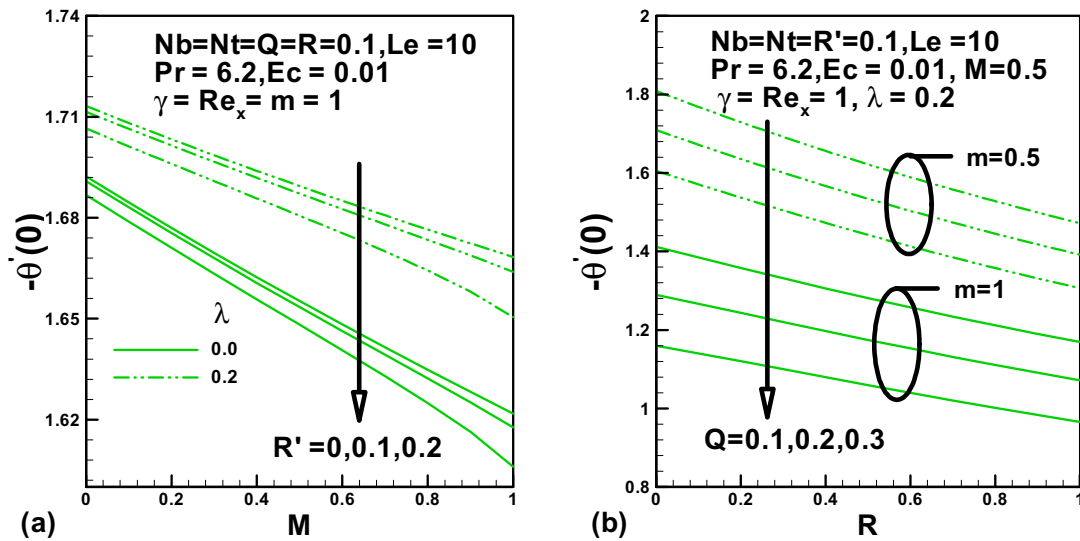


Fig. 12. Effects of  $M$ ,  $R'$ ,  $\lambda$ ,  $m$ ,  $Q$  &  $R$  on  $-\theta'(0)$ .

In Fig. 2(c), the dimensionless primary velocity distribution is plotted for various values of stretching parameter  $\lambda$ . The stretching parameter is defined as the ratio of the velocity of the flow outside the boundary layer (inviscid flow) to the velocity of the stretching sheet. From the Fig. 2(c), it is clearly seen that as stretching parameter increases the primary velocity also increases gradually.

In Fig. 3(a) and (b), dimensionless secondary velocity distribution is plotted for different values of rotational parameter  $R'$  in the absence and presence of stretching parameter  $\lambda$ . From Fig. 3 (a), it is clear that the secondary velocity decreases initially with an increase in the rotational parameter but it increases significantly after a certain distance  $\eta$  normal to the sheet in the absent of stretching parameter. But from the Fig. 3(b), it is noticed that the secondary velocity decreases gradually as rotational parameter increases in the presence of stretching parameter.

Fig.4(a) and (b) clearly demonstrate that the secondary velocity decreases with an increase in the magnetic field in the absence and presence of stretching parameter  $\lambda$ . The magnetic parameter is found to retard the velocity at all points of the flow field. It is

because that the application of transverse magnetic field will result in a resistive type force (Lorentz force) similar to drag force which tends to resist the fluid flow and thus reducing its velocity. Also the boundary layer thickness decreases with an increase in the magnetic field.

Fig. 5(a) shows the effect of magnetic parameter  $M$  on temperature profiles. As shown in the figure magnetic parameter  $M$  increases, temperature also increases. Fig. 5(b) depicts the effect of stretching parameter  $\lambda$  on secondary velocity. It is observed that for the increasing values of  $\lambda$ , temperature decreases. Fig. 5(c) illustrates the effect of radiation parameter  $R$  on temperature profiles. As shown in the figure temperature increases as radiation parameter  $R$  increases.

The variation of temperature profiles with rotational parameter  $R'$  is shown in Fig. 6(a). It is observed that an increase in the value of rotational parameter  $R'$  decreases the temperature. Fig. 6(b) explains the effect of constant parameter  $m$  on temperature profiles. It is observed that temperature profile decreases for increasing value of constant parameter  $m$ . The effect of Brownian motion

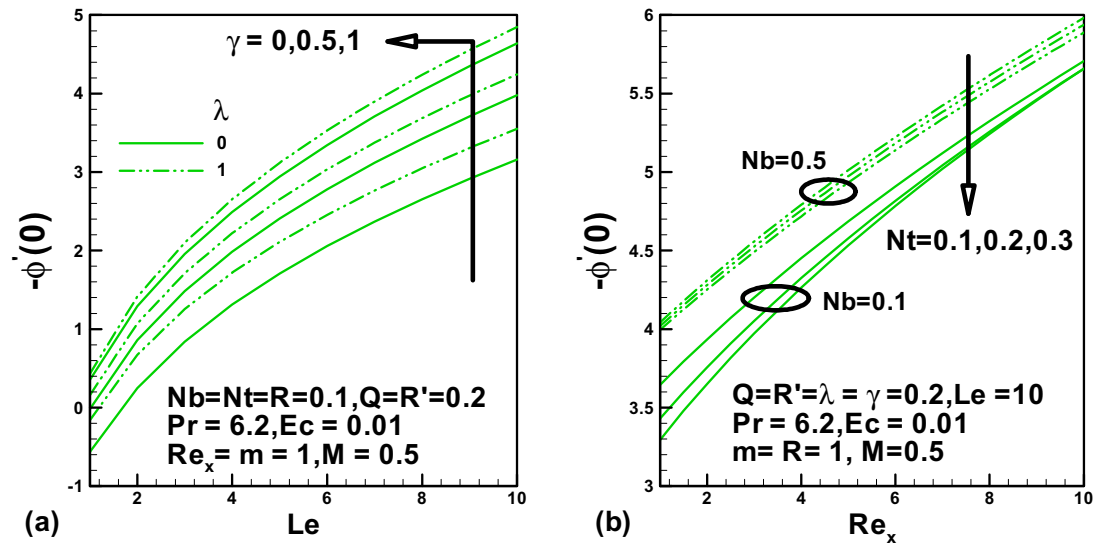


Fig. 13. Effects of  $Le, \gamma, \lambda, Nb, Nt$  &  $Re_x$  on  $-\phi'(0)$ .

$Nb$  on temperature profiles are illustrated in Fig. 6(c). It is clearly observed that temperature increases as Brownian parameter  $Nb$  increases.

The effect of Thermophoresis parameter  $Nt$  on temperature is shown in Fig. 7(a). From these plots, it is observed that the effect of increasing values of  $Nt$  increases temperature profiles. Fig. 7(b) depicts the effect of heat source parameter  $Q$  on temperature profiles. It is noticed that an increase in the heat source parameter  $Q$  increases the temperature profiles of the flow. Fig. 7(c) is plotted to explain the effect of viscous dissipation  $Ec$  on temperature. From these plots, it can be seen that temperature increases with  $Ec$ .

Fig. 8(a) is drawn to illustrate the influence of magnetic parameter  $M$  on concentration profiles. As shown in the figure concentration increases with magnetic parameter  $M$ . Fig. 8(b) reveals that the concentration profiles increases with stretching parameter  $\lambda$ . Fig. 8(c) shows the effect of constant parameter  $m$  on concentration profiles. The figure clearly shows a decrease in dimensionless concentration with an increase in  $m$ .

Fig. 9(a) presents the effect of Lewis number  $Le$  on concentration profiles. As shown in the figure concentration decreases with  $Le$ . Fig. 9(b) shows the concentration profiles for different values of heat source parameter  $Q$ . We infer from this figure that the concentration decreases with an increase in  $Q$ . Fig. 9(c) illustrates the influence of chemical reaction parameter  $\gamma$  on concentration profiles. We have seen a raise in the concentration with an increase in the chemical reaction parameter  $\gamma$ .

Fig. 10(a) represents the effect of Brownian parameter  $Nb$  on concentration profiles. It is evident from the figure that an increase in the Brownian parameter  $Nb$  declines the concentration profiles. Fig. 10(b) reveals the effect Thermophoresis parameter  $Nt$  on concentration profiles of the flow. It is observed that an increase in the Thermophoresis parameter  $Nt$  decreases the concentration profiles of the flow. Fig. 10(c) plotted over concentration profiles for different values of local Reynolds number  $Re_x$ . It is observed that as the of local Reynolds number  $Re_x$  increases, concentration profiles decreases.

Fig. 11(a) depicts the primary shear stress ( $-f''(0)$ ) for different values of rotational parameter  $R'$  and stretching parameter  $\lambda$  drawn against the magnetic parameter  $M$ . It is observed that as the magnetic parameter  $M$  increases the primary shear stress increases gradually. Fig. 11(b) illustrates the secondary shear stress ( $-g'_0(0)$ ) for different values of rotational parameter  $R'$  and stretch-

ing parameter  $\lambda$  drawn against the magnetic parameter  $M$ . It is observed that as the magnetic parameter  $M$  increases the secondary shear stress increases gradually.

Fig. 12(a) shows the dimensionless heat transfer rate  $-\theta'(0)$  for different values of rotational parameter  $R'$  and stretching parameter  $\lambda$  drawn against the magnetic parameter  $M$ . It is noticed that as the magnetic parameter  $M$  increases the dimensionless heat transfer rate decreases. Fig. 12(b) shows the dimensionless heat transfer rate  $-\theta'(0)$  for different values of heat source parameter  $Q$  and constant parameter  $m$  drawn against the radiation parameter  $R$ . It is noticed that as the radiation parameter  $R$  increases the dimensionless heat transfer rate decreases.

Fig. 13(a) presents the dimensionless mass transfer rate  $-\phi'(0)$  for different values of stretching parameter  $\gamma$  and chemical reaction parameter  $\gamma$  drawn against the Lewis number  $Le$ . It is noticed that as the Lewis number  $Le$  increases the dimensionless mass transfer rate increases. Fig. 13(b) shows the dimensionless mass transfer rate  $-\phi'(0)$  for different values of Brownian parameter  $Nb$  and thermophoresis parameter  $Nt$  drawn against the local Reynolds number  $Re_x$ . It is noticed that as the local Reynolds number  $Re_x$  increases the dimensionless mass transfer rate decreases.

The results for  $-f''(0)$  and  $-\theta'(0)$  obtained in the present work and those by Mabood et al. [18] are given in Table 1, for different values of  $Q$  &  $M$ . Table 2 shows the comparative values of  $-\theta'(0)$  with Sreenivasulu and Reddy [25] and Hamad and Pop [26] for different values of  $Pr$ . Moreover, Table 3 also shows the comparative values of  $-\theta'(0)$  with Khan and Pop [22] for various values of  $Nb$  and  $Nt$ .

### 5. Conclusions

In this article, effects of chemical reaction and viscous dissipation on MHD radiative nanofluid over a stretching sheet have been investigated numerically. The problem is studied by transforming the governing equations in nonlinear coupled ordinary differential equations and then solved numerically. The numerical comparison is also presented and found that the present results are in good agreement with the existing literature. The major outcomes for the present analysis are summarized below:

- Large values of thermal radiation parameter and thermophoresis parameter enhance the temperature profile.

- Temperature profile decreases due to the influence of Prandtl number while heat source parameter enhances the temperature profile.
- An increment in Lewis number shows a decrement in concentration profile.
- Nanoparticle volume fraction shows opposite behavior for Brownian motion parameter and thermophoresis parameter.
- The skin friction coefficient increases with the increase of the magnetic field parameter and rotational number.
- The rate of mass transfer increases with the increase of the Lewis number and chemical reaction parameter but a reverse effect occurs for thermophoresis parameter.

## References

- [1] Crane LJ. Flow past a stretching sheet. *J Appl Math Phys* 1970;21:645–7.
- [2] Gupta PS, Gupta AS. Heat and mass transfer on stretching sheet with suction or blowing. *Can J Chem Eng* 1977;55:744–6.
- [3] Rajagopal KR, Na YT, Gupta AS. Flow of a viscoelastic fluid over a stretching sheet. *Rheol Acta* 1984;23:213–5.
- [4] Char MI. Heat and mass transfer in a hydromagnetic flow of the viscoelastic fluid over a stretching sheet. *J Math Anal Appl* 1994;186:674–9.
- [5] Raptis A. Radiations and viscoelastic flow. *Commun Heat Mass Transfer* 1999;26:889–95.
- [6] Abd El-Aziz M. Radiation effect on the flow and heat transfer over an unsteady stretching sheet. *Int Commun Heat Mass Transfer* 2009;36:521–4.
- [7] Shateyi S, Motsa SS. Thermal radiation effects on heat and mass transfer over an unsteady stretching sheet. *Math Prob Eng* 2009;1–13.
- [8] Apelbate A. Mass transfer with a chemical reaction of first order: analytical solutions. *Chem Eng J* 1980;19:19–37.
- [9] Cortell R. MHD flow and mass transfer of an electrically conducting fluid of second grade in a porous medium over a stretching sheet with chemically reactive species. *Chem Eng Proc* 2007;46:721–8.
- [10] Anjalidevi SP, Kandasamy R. Effects of a chemical reaction heat and mass transfer on MHD flow past a semi infinite plate. *J Appl Math Mech* 2000;80:697–701.
- [11] Ibrahim SM, Gangadhar K, Bhaskar Reddy N. Radiation and mass transfer effects on MHD oscillatory flow in a channel filled with porous medium in the presence of chemical reaction. *J Appl Fluid Mech* 2015;8:529–37.
- [12] Mabood F, Khan WA, Ismail AIM. MHD stagnation point flow and heat transfer impinging on stretching sheet with chemical reaction and transpiration. *Chem Eng J* 2015;273:430–7.
- [13] Grebhart B, Mollendorf J. Viscous dissipation in external natural convection flows. *J Fluid Mech* 1969;38:97–101.
- [14] Vajravelu K, Handjinicolaou A. Heat transfer in a viscous fluid over a stretching sheet with viscous dissipation and internal heat generation. *Int Commun Heat Mass Transfer* 1993;20:417–30.
- [15] Wahiduzzaman M, Khan MS, Biswas P, Karim I, Uddin MS. Viscous dissipation and radiation effects on MHD boundary layer flow of a nanofluid past a rotating stretching sheet. *Appl Math* 2016;6:547–67.
- [16] Choi SUS. Enhancing thermal conductivity of fluids with nanoparticles. *Proc ASME Int Mech Eng Cong Expost* 1995;66:99–105.
- [17] Buongiorno J. Connective transport in nanofluids. *J Heat Transfer* 2006;128:240–50.
- [18] Mabood F, Khan WA, Ismail AIM. Approximate analytical modelling of heat and mass transfer in hydromagnetic flow over a non-isothermal stretched surface with heat generation/absorption and transpiration. *J Taiwan Inst Chem Eng* 2015;54:11–9.
- [19] Rana P, Bhargava R. Flow of nanofluid over a nonlinearly stretching sheet. *Commun Nonlinear Sci Numer Simul* 2012;17:212–26.
- [20] Kumar H. Radiative heat transfer with hydromagnetic flow and viscous dissipation over a stretching surface in the presence of variable heat flux. *Therm Sci* 2009;13:163–9.
- [21] Ramana Reddy JV, Sugunamma V, Sandeep N, Sulochana C. Influence of chemical reaction, radiation and rotation on MHD nanofluid flow past a permeable flat plate in porous medium. *J Nigerian Math Soc* 2016;35:48–65.
- [22] Khan WA, Pop I. Boundary-layer flow of a nanofluid past a stretching sheet. *Int J Heat Mass Transfer* 2010;53:2477–83.
- [23] Ferdows M, Khan MS, Alam MM, Sun S. MHD mixed convective boundary layer flow of a nanofluid through a porous medium due to an exponentially stretching sheet. *Math Prob Eng* 2012:408528.
- [24] Ferdows M, Khan MS, Bég OA, Azad MAK, Alam MM. Numerical study of transient magnetohydrodynamic radiative free convection nanofluid flow from a stretching permeable surface. *J Proc Mech Eng* 2013;228:181–96.
- [25] Sreenivasulu P, Reddy NB. Thermal radiation and chemical reaction effects on MHD stagnation-point flow of a nanofluid over a porous stretching sheet embedded in a porous medium with heat absorption/generation: Lie Group Analysis. *J Glob Res Math Arch* 2013;1:13–27.
- [26] Hamad MAA, Pop I. Scaling transformations for boundary layer flow near the stagnation-point on a heated permeable stretching surface in a porous medium saturated with a nanofluid and heat generation/absorption effects. *Transp Porous Media* 2011;87(1):25–39.
- [27] Mabood F, Mastroberardino A. MHD convective flow of a nanofluid over a stretching sheet with viscous dissipation and second order slip. *J Taiwan Inst Chem Eng* 2015;57:62–8.
- [28] Sheikholeslami M, Ganji DD, Javed MY, Ellahi R. Effect of thermal radiation on magnetohydrodynamics nanofluid flow and heat transfer by means of two phase model. *J Magn Magn Mater* 2015;374:36–43.
- [29] Sheikholeslami M, Rashidi MM, Ganji DD. Effect of non-uniform magnetic field on forced convection heat transfer of Fe<sub>3</sub>O<sub>4</sub> water nanofluid. *Comput Methods Appl Mech Eng* 2015;294:299–312.
- [30] Rashidi MM, Ali M, Freidoonimehr N, Rostami B, Hossain MA. Mixed convective heat transfer for MHD viscoelastic fluid flow over a porous wedge with thermal radiation. *Adv Mech Eng* 2014;6:735939.
- [31] Sheikholeslami M, Hayat T, Alsaedi A. MHD free convection of Al<sub>2</sub>O<sub>3</sub>–water nanofluid considering thermal radiation: a numerical study. *Int J Heat Mass Transfer* 2016;96:513–24.
- [32] Mabood F, Khan WA. Analytical study for unsteady nanofluid MHD flow impinging on heated stretching sheet. *J Mol Liq* 2016;219:216–23.
- [33] Imtiaz M, Hayat T, Alsaedi A, Hobiny A. Homogeneous-heterogeneous reactions in MHD flow due to an unsteady curved stretching surface. *J Mol Liq* 2016;221:245–53.